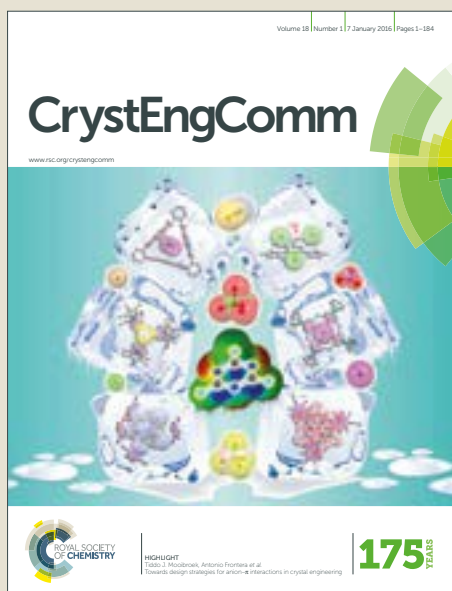


CrystEngComm

Accepted Manuscript



This article can be cited before page numbers have been issued, to do this please use: A. Voronin, T. V. Volkova, A. B. Ilyukhin, T. Trofimova and G. L. Perlovich, *CrystEngComm*, 2018, DOI: 10.1039/C8CE00426A.



This is an Accepted Manuscript, which has been through the Royal Society of Chemistry peer review process and has been accepted for publication.

Accepted Manuscripts are published online shortly after acceptance, before technical editing, formatting and proof reading. Using this free service, authors can make their results available to the community, in citable form, before we publish the edited article. We will replace this Accepted Manuscript with the edited and formatted Advance Article as soon as it is available.

You can find more information about Accepted Manuscripts in the [author guidelines](#).

Please note that technical editing may introduce minor changes to the text and/or graphics, which may alter content. The journal's standard [Terms & Conditions](#) and the ethical guidelines, outlined in our [author and reviewer resource centre](#), still apply. In no event shall the Royal Society of Chemistry be held responsible for any errors or omissions in this Accepted Manuscript or any consequences arising from the use of any information it contains.



Journal Name

ARTICLE

Structural and Energetic aspects of Adamantane and Memantine Derivatives of Sulfonamide Molecular Crystals: Experimental and Theoretical Characterisation

Received 00th January 20xx,
Accepted 00th January 20xx

DOI: 10.1039/x0xx00000x

www.rsc.org/

Alexander P. Voronin^a, Tatiana V. Volkova^a, Andrey B. Ilyukhin^b, Tatiana P. Trofimova^{c,d} and German L. Perlovich^{a,*}

A number of new sulfonamide compounds with adamantane and memantine fragments were synthesised and characterised. Their single crystals were grown and crystal structures were determined. XPac analysis has revealed three sets of isostructural crystals based on adamantane/memantine-specific hydrogen bond patterns. The use of QTAIMC and Hirshfeld surface analysis allowed elucidating the influence of functional groups and molecular arrangement on the strength of inter- and intramolecular non-covalent interactions in crystals and overall packing efficiency. It was found that bulky memantine fragment hinders the formation of C(4) hydrogen-bonded chains, leading to formation of dimeric structures with lower stabilisation energy. The layered packing of hydrophobic fragments in the group of isostructural crystals was found to be the most effective for a group of adamantane derivatives of P2₁/c symmetry.

Introduction

Drug compounds including sulfonamide and/or adamantane/memantine moieties are an important group of biologically active agents for different pathologies. Such compounds demonstrate antibacterial,¹ anticancer,² antithyroid,³ hypoglycemic,^{4,5} antimicrobial,^{5,6} diuretic^{7,8}, antiviral⁹ activity, and also inhibit carbonic anhydrase and protease.^{7,10-13} The search for new drugs in the adamantane series is ongoing and important information devoted to the study of the pharmacological properties, mechanism of action, clinical application, marketing study,¹⁴ and developing the delivery systems based on incorporating the adamantane derivatives¹⁵ has been accumulated by now. For example, an

extensive review on the biological activity of adamantane containing mono- and polycyclic pyrimidine derivatives was published by Shokova and Kovalev¹⁶, and Liu et al.¹⁷ discussed 38 types of adamantane-containing compounds and makes an attempt to elucidate the role of the adamantane moiety on the manifestation of pharmacological activity.

At the same time, the crystallographic studies aimed at clarification of the crystal structure of newly synthesised adamantane derivatives are also represented in the literature. Al-Wahaibi et al.⁵ described the structures of the synthesised adamantane-isothiourea hybrid derivatives by single X-ray crystallographic data. In the study of Saeed et al.¹⁸ the Hirshfeld surface analysis was applied to perform a detailed analysis of the intermolecular interactions in a series of six closely related phenyl thiourea species bearing the 1-(adamantane-1-carbonyl)group. A detailed description of crystal properties including molecular conformational states, packing architecture, and hydrogen bond networks of a number of newly synthesised sulfonamides^{19,20} and adamantanes²¹ using graph set notations was published by Perlovich et al. and the influence of various molecular fragments on the investigated parameters was emphasised.

The crystal structure, thermophysical and thermodynamic properties of molecular crystals of sulfonamide derivatives with an adamantane fragment are described only in several works.^{21,22} Published results show that the work on the synthesis and study of compounds of this class is necessary and will contribute to the development of a scientific strategy for the advancement of compounds with improved pharmaceutical properties from a wide range of structural analogues and will enable the derivation of structure-property

^aG.A. Krestov Institute of Solution Chemistry, Russian Academy of Sciences, 153045 Ivanovo, Russia.

^bInstitute of General and Inorganic Chemistry RAS, 119991 Moscow, Russia.

^cInstitute of Physiologically Active Compounds, Russian Academy of Sciences, 142432, Chernogolovka, Russia.

^dLomonosov Moscow State University, Faculty of Chemistry, 119991 Moscow, Russia

* To whom correspondence should be addressed:

Telephone: +7-4932-533784; Fax: +7-4932-336237; E-mail glp@isc-ras.ru

Electronic Supplementary Information (ESI) available: CCDC links for crystal structures of compounds 4-10. ¹H NMR, ¹³C NMR and IR spectra for compounds 5-10. ORTEP diagrams for crystals of 4-10. Molecular packing of crystals 2, 3, 11, 12, 14. Selected XPac plots of δ_p against δ_a for three sets of isostructural crystals. An XPac map of unique pairs of crystal structures. A sample image and plot of energies of intramolecular C-H...O and C-H... π contacts against the angle between phenyl and adamantane fragments. Correlation plots between the N...O distance, minimal d_{norm} values and hydrogen bond energies evaluated using Mayo force field and QTAIMC. 2D fingerprint plots of Hirshfeld surfaces. Numbering of carbon atoms used in assignment of ¹³C NMR chemical shifts. A scheme of atoms chosen as common set of points for XPac analysis. Lists of unique non-covalent interactions found by QTAIMC in crystal structures of 1-12, 14 with tabulated metric and charge-density properties. See DOI: 10.1039/x0xx00000x

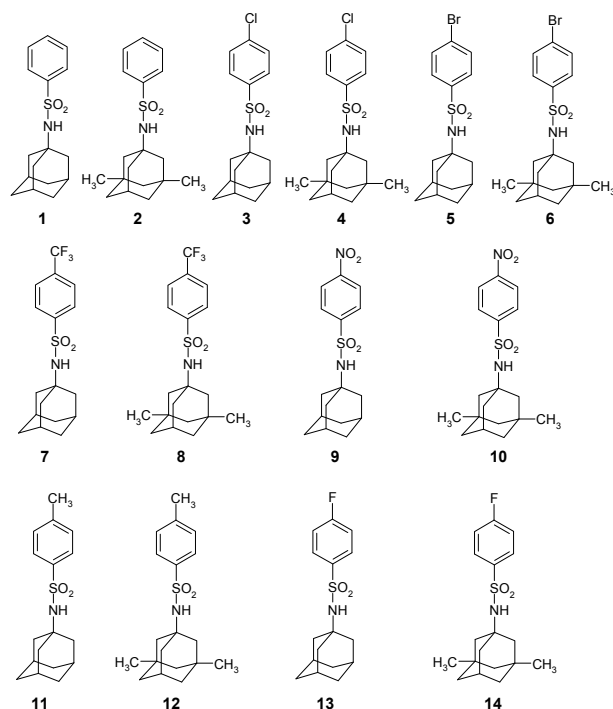


Figure 1. Structural formulae of compounds studied.

relationships with high correlation coefficients.

Our previous work²¹ studied the structures, packing architecture, topology of hydrogen bond networks, and sublimation of 7 adamantane derivatives of sulfonamide. As a continuation of the study, this work focuses on the comparative analysis of the published compounds with new ones: N-Adamantan-1-yl-4-bromo-benzenesulfonamide (5), N-(3,5-Dimethyl-adamantan-1-yl)-4-bromo-benzenesulfonamide (6), N-Adamantan-1-yl-4-trifluoromethyl-benzenesulfonamide (7), N-(3,5-Dimethyl-adamantan-1-yl)-4-trifluoromethyl-benzenesulfonamide (8), N-Adamantan-1-yl-4-nitro-benzenesulfonamide (9), and N-(3,5-Dimethyl-adamantan-1-yl)-4-nitro-benzenesulfonamide (10) (Figure 1). The hydrogen-bonding properties of named compounds are limited by the presence of bulky hydrocarbon fragments, allowing one to study the interplay of interactions which govern the molecular arrangement and packing efficiency in crystal. Hence, the aim of the present investigation was to analyse the influence of substituent nature and molecular topology on the molecule conformational state and the formation of crystal lattice architecture using a variety of topology-based computational approaches.

Experimental

2.1 Synthesis and identification

2.1.1 General procedure of the synthesis of the compounds studied. Synthesis of the novel sulfonamide derivatives was carried out according to Scheme 1.

Triethylamine (0.04 mol) was added to a stirred suspension of 1-aminoadamantane (**I**) (or Memantine, $R^1, R^2 = \text{CH}_3$) (0.01 mol) in isopropanol (30 ml) at 0°C, followed by solid sulfonyl chloride (**II**) ($R^3 = \text{NO}_2, \text{Br}, \text{CF}_3$) (0.01 mol) over a period of 30 minutes. The reaction mixture was heated at 60°C for 2 hours, after which HPLC showed that there was no starting material left. The resulting suspension was cooled to room temperature and the precipitate of triethylamine hydrochloride was removed by filtration. The filtrate was evaporated to dryness to afford colourless oil which was dissolved in ethyl acetate (50 ml), washed with 0.5N HCl (50 ml), water (50 ml) and dried over MgSO_4 . The solvent was evaporated by a rotary evaporator to afford sulfonamide as a white crystalline solid. Yields: 80-90%.

The synthesis procedure of compounds (**1**) – (**4**) and (**11**) – (**14**) was described in our previous papers.^{21,22}

The compounds were carefully purified by re-crystallizing from water-ethanol solution. The precipitate was filtered and dried at room temperature under vacuum until the mass of compounds remained constant. The outlined procedure was repeated several times and the product checked by NMR after each re-crystallisation step until the proton NMR signal correspondence to the purity of the compound over 98-99%.

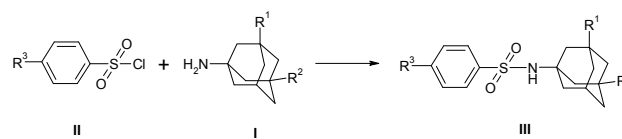
2.1.2 Identification of compounds. ^1H NMR spectra were recorded on Bruker CXP-200 instrument (Germany) with CDCl_3 used as a solvent. Solid-state FT-IR spectra were obtained using the Vertex 80v spectrometer (Germany) in the wavenumber range of $400\text{ cm}^{-1} - 4000\text{ cm}^{-1}$ at 2 cm^{-1} spectral resolution. Differential scanning calorimetry (DSC) was carried out using a Perkin-Elmer DSC 4000 differential scanning calorimeter (USA). DSC runs were performed in a flow of dry nitrogen ($20\text{ ml}\cdot\text{min}^{-1}$) using standard aluminium sample pans at a heating rate of $10\text{ K}\cdot\text{min}^{-1}$.

The ^1H and ^{13}C NMR spectra for newly synthesised compounds **5-10** are presented in Figures 1SI and 2SI, respectively. DSC curves of fusion processes are shown in Figure 3SI, and FT-IR spectra are presented in Figure 4SI. The numeration of carbon atoms used for the band assignment from the ^{13}C spectra is presented in Scheme 1SI.

N-Adamantan-1-yl-4-bromo-benzenesulfonamide (**5**). ^1H NMR (200 MHz, CDCl_3), δ , ppm: 1.54 (m, 6H, AdH), 1.75 (m, 6H, AdH), 2.00 (br. s., 3H, AdH), 4.82 (br. s., 1H, NH), 7.60 (d, $J = 8.60\text{ Hz}$, 2H, ArH), 7.78 (d, $J = 8.60\text{ Hz}$, 2H, ArH).

^{13}C NMR (50 MHz, δ , CDCl_3): 29.60 ($\text{C}^{14}, \text{C}^{15}, \text{C}^{16}$), 35.94 ($\text{C}^8, \text{C}^9, \text{C}^{10}$), 43.17 ($\text{C}^{11}, \text{C}^{12}, \text{C}^{13}$), 55.55 (C^7), 127.04 (C^1), 128.65 (C^2, C^6), 132.29 (C^3, C^5), 143.29 (C^4).

$T_m = 217.7 \pm 0.2\text{ }^\circ\text{C}$. Yield 81.5%. Found (%): C, 52.03; H, 5.29; N, 3.42. $\text{C}_{16}\text{H}_{20}\text{BrNO}_2\text{S}$. Calculated (%): C, 51.90; H, 5.44; N, 3.78.



Scheme 1. The scheme of synthesis of novel sulfonamides.

***N*-(3,5-Dimethyl-adamantan-1-yl)-4-bromo-benzenesulfonamide (6).**

¹H NMR (200 MHz, CDCl₃), δ, ppm: 0.80 (s, 6H, 2CH₃), 1.08 (s, 2H, AdH), 1.25 (m, 4H, AdH), 1.44 (m, 4H, AdH), 1.60 (m, 2H, AdH), 2.07 (m, 1H, AdH), 5.07 (br. s., 1H, NH), 7.65 (d, *J* = 8.60 Hz, 2H, ArH), 7.80 (d, *J* = 8.60 Hz, 2H, ArH).

¹³C NMR (50 MHz, δ, CDCl₃): 29.93, 30.09 (C¹⁴, C¹⁵, C¹⁶), 32.63 (2CH₃), 41.36, 42.14 (C⁸, C⁹, C¹⁰), 49.14, 50.12 (C¹¹, C¹², C¹³), 56.97 (C⁷), 126.91 (C¹), 128.49 (C², C⁶), 132.18 (C³, C⁵), 143.12 (C⁴).

T_m = 170.6 ± 0.2 °C. Yield 68.3%. Found (%): C, 54.53; H, 6.09; N, 3.44. C₁₈H₂₄BrNO₂S. Calculated (%): C, 54.27; H, 6.07; N, 3.52.

***N*-Adamantan-1-yl-4-trifluoromethyl-benzenesulfonamide (7).**

¹H NMR (200 MHz, CDCl₃), δ, ppm: 1.56 (m, 6H, AdH), 1.76 (m, 6H, AdH), 1.99 (br. s., 3H, AdH), 5.00 (br. s., 1H, NH), 7.74 (d, *J* = 8.06 Hz, 2H, ArH), 8.03 (d, *J* = 8.06 Hz, 2H, ArH).

¹³C NMR (50 MHz, δ, CDCl₃): 29.60 (C¹⁴, C¹⁵, C¹⁶), 35.89 (C⁸, C⁹, C¹⁰), 43.19 (C¹¹, C¹², C¹³), 55.81 (C⁷), 120.77 (C¹), 126.18 (C², C⁶), 127.49 (C³, C⁵), 133.89 (CF₃), 147.73 (C⁴).

T_m = 197.7 ± 0.2 °C. Yield 86.5%. Found (%): C, 56.53; H, 5.49; N, 3.62. C₁₇H₂₀F₃NO₂S. Calculated (%): C, 56.81; H, 5.61; N, 3.90.

***N*-(3,5-Dimethyl-adamantan-1-yl)-4-trifluoromethyl-benzenesulfonamide (8).**

¹H NMR (200 MHz, CDCl₃), δ, ppm: 0.79 (s, 6H, 2CH₃), 1.08 (s, 2H, AdH), 1.24 (m, 4H, AdH), 1.45 (m, 4H, AdH), 1.61 (m, 2H, AdH), 2.08 (m, 1H, AdH), 4.83 (br. s., 1H, NH), 7.76 (d, *J* = 8.32 Hz, 2H, ArH), 8.03 (d, *J* = 8.32 Hz, 2H, ArH).

¹³C NMR (50 MHz, δ, CDCl₃): 29.99, 30.22 (C¹⁴, C¹⁵, C¹⁶), 32.78 (2CH₃), 41.41, 42.21 (C⁸, C⁹, C¹⁰), 49.28, 50.19 (C¹¹, C¹², C¹³), 57.33 (C⁷), 120.74 (C¹), 126.16 (C², C⁶), 127.46 (C³, C⁵), 133.97 (CF₃), 147.66 (C⁴).

T_m = 111.6 ± 0.2 °C. Yield 87.5%. Found (%): C, 58.63; H, 6.09; N, 3.42. C₁₉H₂₄F₃NO₂S. Calculated (%): C, 58.90; H, 6.24; N, 3.61.

***N*-Adamantan-1-yl-4-nitro-benzenesulfonamide (9).**

¹H NMR (200 MHz, CDCl₃), δ, ppm: 1.60 (m, 6H, AdH), 1.81 (m, 6H, AdH), 2.04 (br. s., 3H, AdH), 4.76 (br. s., 1H, NH), 8.10 (d, *J* = 8.80 Hz, 2H, ArH), 8.35 (d, *J* = 8.80 Hz, 2H, ArH).

¹³C NMR (50 MHz, δ, CDCl₃): 29.58 (C¹⁴, C¹⁵, C¹⁶), 35.85 (C⁸, C⁹, C¹⁰), 43.23 (C¹¹, C¹², C¹³), 56.08 (C⁷), 124.41 (C², C⁶), 128.00 (C¹), 128.30 (C³, C⁵), 149.90 (C⁴).

T_m = 226.2 ± 0.2 °C. Yield 80.7%. Found (%): C, 57.42; H, 5.69; N, 8.42. C₁₆H₂₀N₂O₄S. Calculated (%): C, 57.13; H, 5.99; N, 8.33.

***N*-(3,5-Dimethyl-adamantan-1-yl)-4-nitro-benzenesulfonamide (10).**

¹H NMR (200 MHz, CDCl₃), δ, ppm: 0.80 (s, 6H, 2CH₃), 1.09 (s, 2H, AdH), 1.26 (m, 4H, AdH), 1.46 (m, 4H, AdH), 1.62 (m, 2H, AdH), 2.08 (m, 1H, AdH), 5.12 (br. s., 1H, NH), 8.08 (d, *J* = 8.60 Hz, 2H, ArH), 8.33 (d, *J* = 8.60 Hz, 2H, ArH).

¹³C NMR (50 MHz, δ, CDCl₃): 29.99, 30.22 (C¹⁴, C¹⁵, C¹⁶), 32.81 (2CH₃), 41.54, 42.17 (C⁸, C⁹, C¹⁰), 49.31, 50.15 (C¹¹, C¹², C¹³), 57.63 (C⁷), 124.39 (C², C⁶), 127.01 (C¹), 128.26 (C³, C⁵), 149.84 (C⁴).

T_m = 159.6 ± 0.2 °C. Yield 88.5%. Found (%): C, 59.53; H, 6.49; N, 7.42. C₁₈H₂₄N₂O₄S. Calculated (%): C, 59.32; H, 6.64; N, 7.69.

2.2 Single crystals preparation

Single crystals of compounds 4-10 were grown from 96% ethanol by slow evaporation. A powder sample of the substance was fully dissolved at room temperature to yield a clear solution. The solution was filtered through a 0.22 μm PTFE syringe filter into a glass vial, then the vial was sealed by Parafilm[®] with few small holes pierced and the solvent was allowed to evaporate at room temperature for 3-5 days. For compound 13, one did not manage to obtain the diffraction quality crystals of sufficient size using this method.

2.3 X-ray diffraction experiments

Experimental data from single crystals 5, 7-10 were obtained on a Bruker SMART APEX2 diffractometer²³ (Table 1). Absorption for 1, 3 and 4 was taken into account by a semi-empirical method based on equivalents using SADABS software²⁴. Experimental data from single crystals 4 and 6 were obtained on a Bruker Oxford Diffraction Xcalibur diffractometer²⁵ (Table 1). Absorption for 4 and 6 was taken into account by a semi-empirical method based on equivalents using *CrysAlis RED* software.²⁵ The structures were determined using a combination of the direct method and Fourier syntheses. All the calculations were carried out using SHELXL-2016 software.²⁶

2.4 Calculation procedure

2.4.1 Free molecular volume calculation. The free molecular volume in the crystal lattice was estimated on the basis of the X-ray diffraction data and van-der-Waals molecular volume (*V^{vdw}*), calculated by GEPOL:²⁷

$$V^{free} = (V_{cell} - Z \cdot V^{vdw}) / Z \quad (1)$$

where *V_{cell}* is the volume of the unit cell, *Z* is the number of molecules in the unit cell.

2.4.2 XPac analysis. The quantitative analysis of packing similarity was performed using XPac v. 2.0.2.²⁸ This method allows finding the isostructural supramolecular constructs within the pairs of crystals by comparing the relative position and orientation of identical molecular graphs named 'common sets of points' in clusters which imitate the crystal environment of a molecule. The measure of packing similarity is the dissimilarity index *X*, which shows the difference in angles δ_a and interplanar angles δ_p, and stretch parameter *D*, which indicates the difference in distances between the nearest identical fragments. Lattice parameters and positions of all heavy atoms used in the calculation were taken from the X-Ray experiment. A cluster of 15 molecules with intermolecular atom-atom distance shorter than sum of van-der-Waals radii of contact atoms + 1.5 Å was considered for each crystal. Medium-level threshold values for parameters δ_a and δ_p were used, which equals 10° and 14°, respectively.

2.4.3 Hydrogen bond energy calculation. The hydrogen bonding energy was calculated with the help of Mayo et al.²⁹ force field:

$$E_{HB} = D_{HB} \cdot [5(R_{hb} / R_{DA})^{12} - 6(R_{hb} / R_{DA})^{10}] \cdot \cos^4(\theta_{DHA}) \quad (2)$$

where $D_{HB} = 39.7 \text{ kJ}\cdot\text{mol}^{-1}$ is a depth of potential well of pair potential at creation of hydrogen bond of H_2O dimer; $R_{hb}=2.75 \text{ \AA}$; R_{DA} , θ_{DHA} are the distance and angle between donor and acceptor atoms.

2.4.4 Solid-state DFT calculations followed by QTAIMC analysis of periodic electron density. Density functional theory computations with periodic boundary conditions (solid-state DFT) were performed in the CRYSTAL14 software package³⁰ using meta-GGA B3LYP functional in localised 6-31G(d,p) basis set. The B3LYP/6-31G(d,p) approximation was proven to provide reliable and consistent results in studying the intermolecular interactions in crystals.³¹ Since dispersive interactions are supposed to contribute significantly into the stability of the crystal lattice, the D2 empirical correction by Grimme et al. was used in periodic wavefunction calculations.³² The unit cell parameters and positions of heavy atoms determined with high accuracy from low-temperature X-Ray diffraction experiment were fixed, while the coordinates of hydrogen atoms were optimised for all structures. Bader analysis³³ of periodic electron density, or QTAIMC³⁴ was performed in TOPOND14,³⁵ and search for (3;-1) critical points was conducted between the pairs of atoms within the 5 Å radius around each symmetry-inequivalent atom in unit cell. The following electron-density features at the bond critical point were computed for every non-covalent interaction: (i) the values of the electron density, ρ_b , (ii) the Laplacian of the electron density, $\nabla^2\rho_b$, and (iii) the positively defined local electronic kinetic energy density, G_b . The threshold on ρ_b for considered interactions was set as 0.003 a.u. since weaker interactions are too small for determination by existing experimental and computational methods.³⁴ The energy of the particular single non-covalent interaction E_{int} was estimated using the equation proposed by Mata et al.:³⁶

$$E_{int}(\text{kJ}\cdot\text{mol}^{-1}) = 1147 \cdot G_b(\text{a.u.}) \quad (3)$$

Equation (7) yields reasonable E_{int} values for molecular crystals with different types of intermolecular interactions: H-bonds, C-H...O, H...H and π -stacking contacts, etc.³⁷ Total cohesion energy³⁸ was calculated as sum of energies of all intermolecular interactions in the asymmetric unit as described elsewhere:

$$E_{latt} = \sum_i \sum_{j < i} E_{int,j,i} \quad (4)$$

where $E_{int,j,i}$ is the energy of a particular non-covalent interaction. Indices j and i denote the atoms belonging to different molecules. The presented approach provides reasonable values for single-component³⁹ and two-component^{40,41} molecular crystals.

2.4.5 Hirshfeld surface analysis. The analysis of Hirshfeld surfaces⁴² of molecules within the crystal was performed in *CrystalExplorer v.3.1*.⁴³ The surface resolution was set to 'Very High'. The distances from the Hirshfeld surface to the nearest nucleus outside and inside the surface (d_e and d_i , respectively) were plotted into a 2D fingerprint map. The contributions from

interactions between atoms of different types into the surface were calculated basing on the normalised distance of intermolecular contact d_{norm} ⁴⁴ between different pairs of nuclei calculated as:

$$d_{norm} = \frac{d_i - r_i^{vdW}}{r_i^{vdW}} + \frac{d_e - r_e^{vdW}}{r_e^{vdW}} \quad (5)$$

Here r_i and r_e are the van-der-Waals radii of contact atoms inside and outside the Hirshfeld surface.

Results and Discussion

3.1 Crystal structure analysis

The results of X-ray diffraction experiments are presented in Table 1. The numbering of atoms of the considered compounds was unified and exemplified by compound 3 (Figure 2). Hydrogen bond geometry and graph set notations of the studied molecules are summarised in Table 2. Thermal ellipsoids for compounds 4-10 are shown in Figure S5I.

It would be also interesting to compare the molecular packing motifs in studied crystals and in the crystals of structurally similar compounds. For this purpose, we used a row of thiourea derivatives reported by Saeed et al.^{18,45-47} and Al-Wahaibi et al.⁵ and a number of adamantane-based carboxamides reported by various groups and extracted from Cambridge Structural Database. The crystallographic data and CSD refcodes for these compounds are listed in Table 1SI. Of these crystals, 16 adamantane-substituted carboxamides form C(4), compared to only two structures (VICHAR and VUXCOI) from this row with dimer organization. However, in case of structurally different adamantane derivatives of thiourea, the various types of ring motifs occur in 10 of 11 crystals. The reasons for this disproportion are clarified below.

The hydrogen bonds of the selected crystals form networks with various topological structures. To analyse the hydrogen bond networks topology, we used graph set notation terminology introduced by Etter⁴⁸ and supplemented by Bernstein.⁴⁹ The comparative characteristics of the hydrogen bonds geometry and matrix of the topological graphs describing hydrogen bond networks topology of the molecular crystals are presented in Table 2. The topological graphs

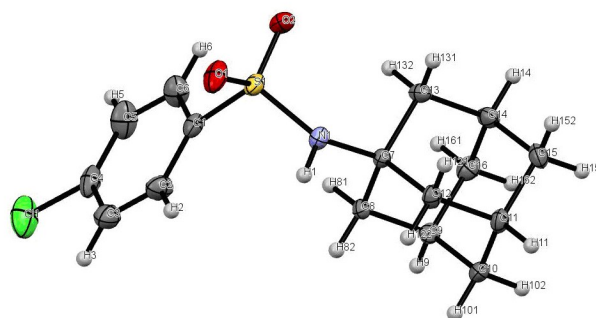


Figure 2. Unified numbering of atoms of the considered compounds (exemplified by compound 3)

Table 1. Crystal data and structure refinement for **4-10**.^a

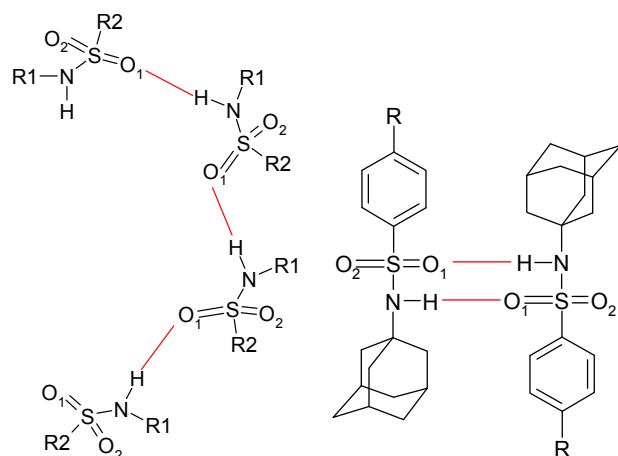
Compound	4	5	6	7	8	9	10
Formula	C ₁₈ H ₂₄ ClNO ₂ S	C ₁₆ H ₂₀ BrNO ₂ S	C ₁₈ H ₂₄ BrNO ₂ S	C ₁₇ H ₂₀ F ₃ NO ₂ S	C ₁₉ H ₂₄ F ₃ NO ₂ S	C ₁₆ H ₂₀ N ₂ O ₄ S	C ₁₈ H ₂₄ N ₂ O ₄ S
CCDC code	1590179	1590180	1590181	1590182	1590183	1590184	1590185
crystal system	monoclinic	monoclinic	monoclinic	monoclinic	monoclinic	monoclinic	monoclinic
space group	P2 ₁ /c	P2 ₁ /c	P2 ₁ /c	C2/c	P2 ₁ /c	P2 ₁ /c	P2 ₁ /c
crystal size, mm	0.30×0.27×0.25	0.4×0.28×0.2	0.38×0.31×0.29	0.36×0.28×0.2	0.4×0.28×0.2	0.4×0.32×0.2	0.3×0.28×0.24
<i>a</i> , Å	10.3869(3)	11.0548(8)	10.5014(3)	29.081(2)	10.7288(4)	11.0672(8)	10.5834(3)
<i>b</i> , Å	15.4759(3)	6.4659(4)	15.4718(4)	6.8576(6)	15.5406(6)	6.4621(5)	15.2084(5)
<i>c</i> , Å	11.2824(3)	21.6540(14)	11.3326(3)	19.1376(16)	11.6218(5)	21.5494(16)	11.6137(3)
β, °	105.723(3)	102.382(2)	106.420(3)	123.701(2)	106.4540(10)	103.132(2)	107.1010(10)
volume, Å ³	1745.75(8)	1511.81(17)	1766.18(9)	3175.1(4)	1858.37(13)	1500.85(19)	1786.66(9)
Z	4	4	4	8	4	4	4
D _{calc} , g·cm ⁻³	1.346	1.627	1.498	1.504	1.385	1.489	1.355
radiation	Mo K _α	Mo K _α	Mo K _α	Mo K _α	Mo K _α	Mo K _α	Mo K _α
T, K	100(1)	150(2)	150(1)	150(2)	150(2)	150(2)	120(2)
μ, mm ⁻¹	0.347	2.861	2.455	0.247	0.216	0.239	0.207
Data collection							
measured reflections	7663	16988	16291	21520	27756	18790	21605
independent reflections	3974	5149	7633	4464	6393	4388	5681
independent reflections with I > 2σ(I)	3243	3856	5678	3495	5285	3378	4776
R _{int}	0.0214	0.0477	0.0225	0.0507	0.033	0.0455	0.0333
Θ _{max} , °	29.18	32.078	35.839	28.87	32.03	30.07	31.51
Refinement							
refinement on	F ²	F ²	F ²	F ²	F ²	F ²	F ²
R1 [F ² > 2σ(F ²)]	0.0370	0.0368	0.0366	0.0687	0.0473	0.0437	0.0394
wR (F ²)	0.0912	0.0968	0.0876	0.1875	0.1435	0.1071	0.115
S	1.044	0.994	0.998	1.277	1.124	1.000	1.018
reflections	3974	5149	7633	4464	6393	4388	5681
parameters	304	270	304	279	309	288	322
(Δ/σ) _{max}	<0.001	0.002	0.002	<0.001	<0.001	<0.001	0.001
Δρ _{max} , e·Å ⁻³	0.333	0.518	0.521	1.224	0.975	0.464	0.486
Δρ _{min} , e·Å ⁻³	-0.384	-0.593	-0.736	-0.409	-0.599	-0.388	-0.337
V ^{vhv} , Å ³	295.9	272.9	302.6	274.8	305.3	269.2	301.8
V ^{free} , Å ³	140.5	105.1	138.9	122.0	159.3	106.0	144.9
B = V ^{free} / V ^{vhv} , %	47.5	38.5	45.9	44.4	52.2	39.4	48.0
K = V ^{vhv} / V _{total} , %	67.8	72.2	68.5	69.2	65.7	71.8	67.6

^a Standard deviations are presented in brackets

occurring in the studied crystals are shown in Scheme 2. According to Table 2, all compounds under study can be divided into three groups. The first group contains compound **1** which does not form N-H...O hydrogen bonds. The second group includes the compounds which form hydrogen-bonded chains with four involved atoms C(4) (**3**, **5**, **7**, **9**, **11**). Compounds with the adamantane fragment excluding **1** belong to this group. Finally, the third group consists of the compounds with dimer organisation of hydrogen bonds (with graph set notation R₂²(8)), which have memantine fragment (**2**, **4**, **6**, **8**, **10**, **12**, **14**) in their structure. We consider that the differences in hydrogen bond motifs are based on steric hindrances that occur in the molecules with the memantine fragment, so methyl groups impede the formation of C(4) infinite chains. The impact of memantine/adamantane substituent on the hydrogen bond topology is confirmed by comparing the crystal structures of compounds consisting only from an adamantane/memantine cage and an alkylamide

group: N-adamantanyl-acetamide⁵⁰ (refcode: ROLCOK01) and N-(dimethyladamantanyl)-formamide⁵¹ (refcode: VICHAR). Even in such a simple system, the difference in hydrogen bond topology is observed: an adamantane derivative forms C(4) H-bonded chains, while an memantine-based compound is packed into centrosymmetric R₂²(8) dimers (Figure 6SI). Note that for crystal VUXCOI⁵² with limited conformational mobility also forms dimers instead of chains.

It would be interesting to analyse whether the hydrogen bonds in chains and dimers differ in strength from one another. In order to compare it, the energies of N-H...O bonds were evaluated using equation (2) (Table 2) as well as using QTAIMC. It was found that the average absolute value of hydrogen bonding energy in chains is somewhat lower than in dimers (10.6 < 15.3 kJ·mol⁻¹). Besides that it should be noted that the energy of hydrogen bond within the chain in compound **11** is unusually low (-2.6 kJ·mol⁻¹) compared to the mean value (-10.6 kJ·mol⁻¹).



Scheme 2. Different hydrogen bond topologies observed in studied crystals: infinite chains (left) and cyclic dimers (right).

3.1.1 Molecular conformational analysis. The conformational states of the investigated molecules depend on the mobility of the sulfonamide link, connecting phenyl rings and adamantane fragment. The torsion angle $\angle C2-C1-S1-N1$ (τ_1) between the SO_2 -group and the phenyl motif Ph (C1-C2-C3-C4-C5-C6) has been chosen to describe the conformational state. Since the bridge atoms are involved into hydrogen bonding, we have attempted to find a correlation between the angle τ_1 and the strength of a corresponding hydrogen bond (E_{HB}). The results are displayed in Figure 3. It is not hard to see that as the hydrogen bond strength gets higher, the τ_1 value decreases. Moreover, τ_1 for the substances that form infinite C(4) chains (red dots) is higher compared to the dimer-forming ($R_2^2(8)$) - black dots.

3.1.2 Packing architecture analysis. As noted above, for convenience, studied compounds can be divided into three groups: compounds without hydrogen bonds (1), those forming infinite chains C(4) (3, 5, 7, 9, 11) and crystals with dimer structure organisation $R_2^2(8)$ (2, 4, 6, 8, 10, 12, 14).

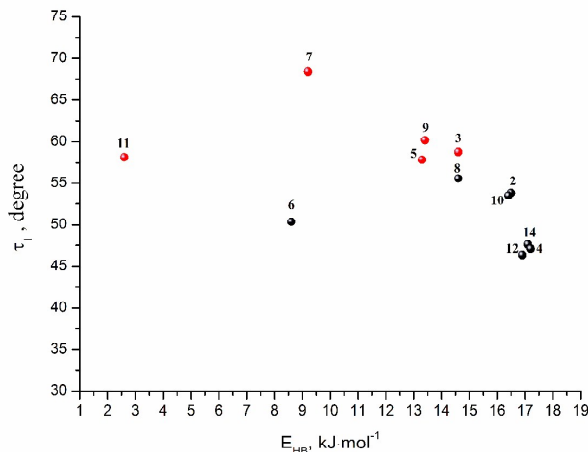


Figure 3. Dependence between τ_1 and hydrogen bond energy (E_{HB}) estimated using equation (2). Numbering corresponds to Figure 1. The red points correspond to the compounds with C(4) hydrogen bonds topology, whereas the black points – the ones with $R_2^2(8)$ topology.

The molecular packing of compounds 3, 5, 7, 9, 11 are very similar to one another. For molecules 3 and 11 they have been already described in one of our previous works²¹ (Figure 7SI a and b). Figure 4 (a, b, c) shows the packing projections for 5, 7, 9. Molecular packing can be presented in the following way. The hydrogen bonds appearing between the sulfonamide bridges form helicoids parallel to (OY)-axis. The centres of the helicoids are located in 1/4 and 3/4 of the (OZ) distance. In turn, the mentioned chains interact with each other in the crystal by van-der-Waals's forces (Figure 4a).

The molecules are packed into layers, one of which being displayed in the (ZOX) plane in Figure 4a. Within the plane, the alternation of pairs of phenyl and adamantane fragments can be distinguished in certain directions. In adjacent directions, the phenyl fragments interact with the same fragment via the pi-stacking from the one side. The substituents in para-

Table 2. Hydrogen bonds geometry, graph set notations and hydrogen bond energies (E_{HB}) in the studied compounds calculated by different methods

	D—H...A ^a [Å]	D—H [Å]	H...A [Å]	D...A [Å]	D—H...A [°]	$-E_{HB(Mayo)}^c$ [kJ·mol ⁻¹]	$E_{HB(QTAIMC)}^d$ [kJ·mol ⁻¹]	Graph set notation
2 ^b	N1-H1...O1 ⁱ	0.932	1.992	2.918	172.4	16.5	22.9	$R_2^2(8)$
3 ^b	N1-H1...O1 ⁱ	0.891	2.073	2.949	167.7	14.6	21.3	C(4)
4 ^b	N1-H1...O1 ⁱ	0.813	2.074	2.880	171.3	17.2	24.9	$R_2^2(8)$
5	N1-H1...O1 ^{iv}	0.83(2)	2.16(2)	2.963(2)	163(2)	13.3	20.1	C(4)
6	N1-H1...O1 ⁱ	0.86(2)	2.13(2)	2.882(2)	146.2	8.6	20.1	$R_2^2(8)$
7	N1-H1...O1 ^v	0.93(3)	2.25(3)	3.136(2)	161(3)	9.2	14.0	C(4)
8	N1-H1...O1 ^{vi}	0.87(2)	2.11(2)	2.9647(15)	168(2)	14.6	20.1	$R_2^2(8)$
9	N1-H1...O1 ⁱⁱ	0.819(19)	2.16(2)	2.9476(18)	162.3(18)	13.4	20.7	C(4)
10	N1-H1...O1 ⁱⁱⁱ	0.857(18)	2.051(18)	2.8975(12)	169.2(17)	16.4	23.8	$R_2^2(8)$
11 ^b	N1-H1...O1 ⁱ	0.860	2.373	3.000	130.1	2.6	12.7	C(4)
12 ^b	N1-H1...O1 ⁱ	0.836	2.070	2.900	172.0	16.9	23.8	$R_2^2(8)$
14 ^b	N1-H1...O1 ⁱ	0.848	2.048	2.891	172.3	17.1	23.9	$R_2^2(8)$

^a Symmetry codes: (i) x,y,z; (ii) -x,y+1/2,-z+1/2; (iii) -x,-y,-z; (iv) -x+1,y+1/2,-z+1/2; (v) -x+1/2,y-1/2,-z+1/2; (vi) -x+1,-y+1,-z+1;

^b Data taken from our earlier work;²¹

^c Calculated by Mayo equation;²⁹

^d Calculated by QTAIMC³⁴ using equation (3).³⁶

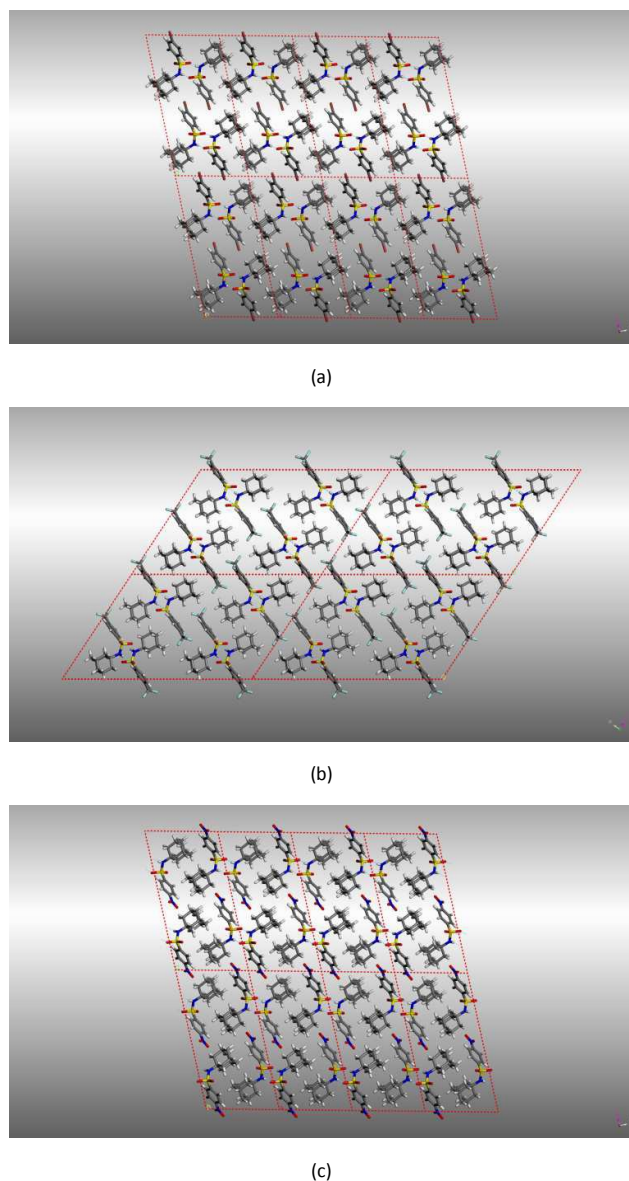


Figure 4. Molecular packing architectures of crystals **5** (a), **7** (b) and **9** (c).

positions are faced in opposite directions above and below the plane of the considered layer. From the other side the phenyl ring forms the close contact with the adamantane fragment stabilised by van-der-Waals interactions. The crystal lattices of **3**, **5**, **9**, **11** are isomorphous within the $P2_1/c$ space group and approximately the same unit cell parameters.

The molecular packing in crystals **2**, **4**, **6**, **8**, **10**, **12**, **14** has several common features. For compounds **2**, **12** and **14** these features have been already described by us earlier²¹ (Figure 8SI a, b and c). Fig. 5 (a, b, c, d) shows the molecular packing projections in compounds **4**, **6**, **8**, **10**.

The dimers of molecules **6** are uniformly packed in the plane (YOZ), i.e. it is not possible to distinguish any anisotropy within the plane. In a projection parallel to (XOZ) the dimers of molecules create alternately interlacing layers, composed of

phenyl and adamantane molecular fragments (Figure 5 b). The adamantane motifs extend from the sulfonamide phenyl fragments of the selected dimer into the adjacent layers (above and below the imaginary plane formed by the phenyl

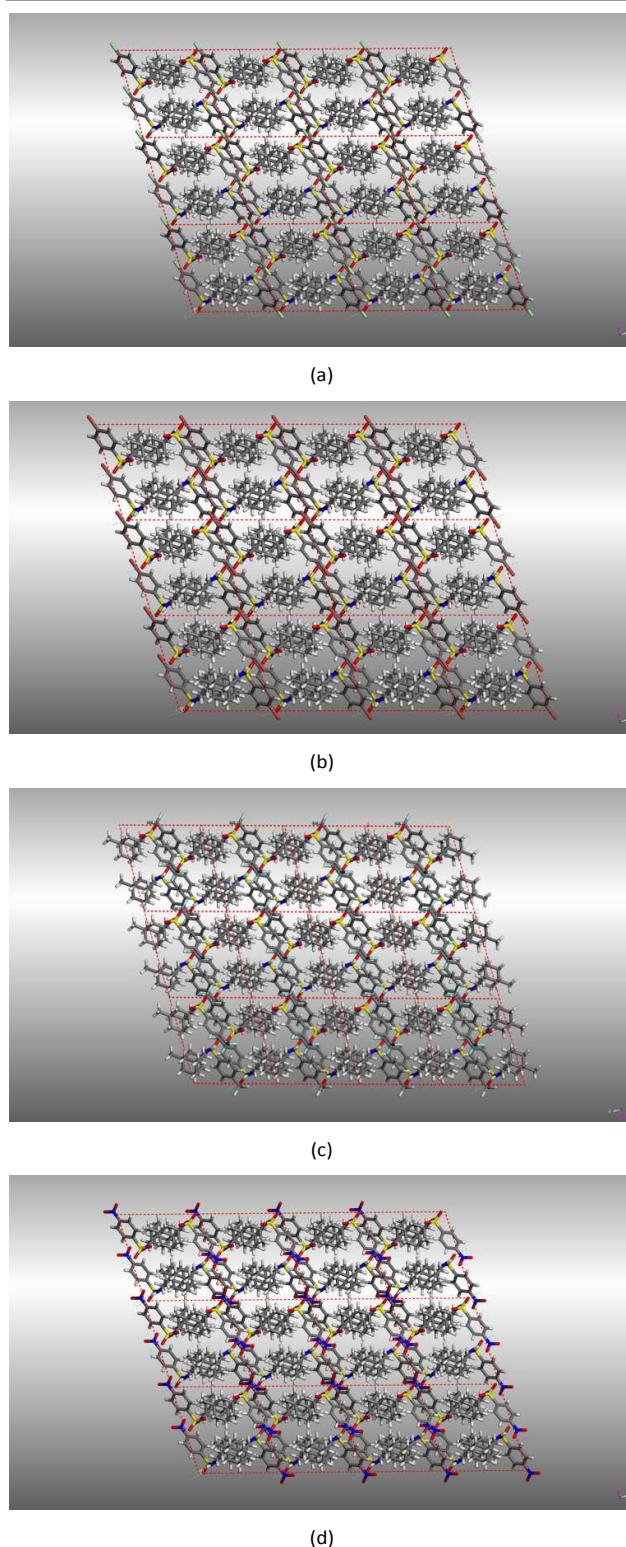


Figure 5. Molecular packing architectures of crystals **4** (a), **6** (b), **8** (c) and **10** (d).

parts of the molecules). In its turn, the “adamantane” layer is composed in such a way that each adamantane motif alternately extends from the layers located above and below. This packing looks like interlaced fingers. Such molecular packing allows us to conclude that crystal growth from dimer saturated solution is carried out by means of delicate adjustment of the adamantane fragments into the corresponding layers. Crystal structure data gives opportunity to calculate a free volume per molecule (V^{free}) in a crystal and analyse molecular packing by using $\beta = V^{free}/V^{vdw}$ parameter. This parameter shows how much the free volume increases as the molecular van-der-Waals volume grows. The value of the discussed parameter depends on the molecular topology, the nature of atoms and the availability of hydrogen bond networks. The experimental value of β -parameter is a result of crystal lattice Gibbs energy minimisation, including both enthalpy and entropy terms. The dependence of the β -parameter on V^{vdw} is shown in Figure 6. The parent compounds of considered rows are the substance **1** with adamantane substituent (red points) and substance **2** with memantine fragment (black points). It is easy to see that the packing densities for most compounds of the second group are significantly lower (i.e. higher β -parameter values) compared to the first group. The only exception is the crystal **6**, for which β -parameter is comparable to compounds **1**, **7**, **11**. Considering the substances within each group, the following dependencies can be traced:

For the first group of compounds, the introduction of bulky fragments $-CF_3$ (**7**) and $-CH_3$ (**11**) into the para-position of the phenyl ring reduce the packing efficiency with respect to the original compound **1**, whereas the substituents $-Cl$ (**3**), $-NO_2$ (**9**) and $-Br$ (**5**) – increase the molecular packing density in crystal (β -parameter decreases). Moreover, for the second subgroup of compounds a linear correlation is observed between β -parameter and V^{vdw} (Fig. 6, blue dotted line).

For the second group of compounds, the presence of any fragment in para-position of the phenyl ring increases the

packing density compared to parent compound **2**: $-CH_3$ (**12**), $-NO_2$ (**10**), $-Cl$ (**4**), $-Br$ (**6**). The exceptions are the fluorine-based functional groups: $-F$ (**14**), $-CF_3$ (**8**). Similar to the first group, a correlation between β -parameter and V^{vdw} is observed for crystals **2**, **4**, **6**, **10** and **12** (Fig. 6, red dotted line).

3.1.3 XPac analysis. The XPac method enables to quantitatively describe the similarity in crystal packing and to provide a basis for the assessment of isostructurality in studied crystals. Moreover, the packing similarity may also indicate the common features in intermolecular interactions and hence, in the thermodynamic properties.

The chosen common set of points for studied compounds includes all heavy atoms of compound **1** with no substituents in molecular structure (see Scheme 2SI). For the dataset of 13 crystal structures under study, a matrix of $[13 \times (13 - 1) / 2] = 78$ unique pairs of crystals was considered and the packing dissimilarity index X and stretch parameter D were investigated for each pair. The results are presented in Figure 7.

As shown in Figures 9SI and Scheme 3, the results of XPac analysis confirm our empirical suggestions of packing similarity. Three sets of crystals with the established 3D isostructurality can be isolated (Figure 10SI a, b and c):

1. A set of adamantane derivatives crystallizing in $P2_1/c$ space group, C(4) hydrogen-bonded chains and layered packing of alternating pairs of adamantane and phenyl fragments.

Compounds **3**, **5**, **9**, **11** belong to this group.

2. A set of memantine derivatives with a large substituent in phenyl ring ($-Cl$, $-Br$, $-NO_2$, $-CF_3$) crystallizing in $P2_1/c$ space group. The features of these crystals are $R_2^2(8)$ dimer structure organisation of hydrogen bonds and interlaced packing of memantine moieties. This group contains compounds **4**, **6**, **8**, **10**.

3. A set of memantine derivatives with small substituent in phenyl ring ($-F$, $-CH_3$) crystallizing in $P2_1/n$ space group. Like in the previous set, the hydrogen bonds form $R_2^2(8)$ dimers. The memantine cages and phenyl rings of adjacent molecules are packed into a chain-like manner via C-H...C close contacts along the a axis. Only two compounds, **12** and **14**, build this group.

Within a row of similarly packed crystals, lowest values of X (which means highest degree of packing similarity) are

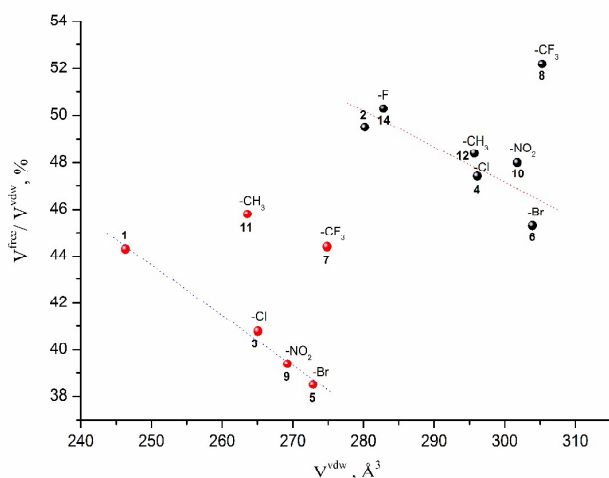
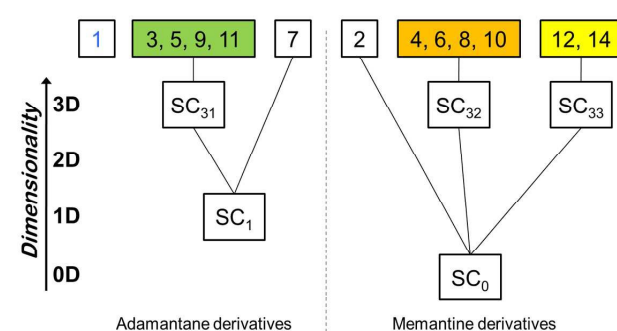


Figure 6. Dependence of β -parameter (V^{free}/V^{vdw}) versus V^{vdw} . The numbering corresponds to Figure 1. Red points correspond to compounds with adamantane fragment, whereas the black points – with memantine fragment.



Scheme 3. Diagram showing the structural relationship between 13 adamantane- and memantine-substituted sulfonamides with crystal structures determined. The numeration used is consistent with Figure 1.

observed for the pairs of structures with the substituent of similar size: -Cl – -CH₃, -Cl – -Br, -CH₃ – -Br, -NO₂ – -CF₃ etc.⁵³

Additionally, some low-degree packing similarity can be traced for all memantine derivatives (hydrogen-bonded dimer organisation – OD supramolecular construct SC₀ in pairs with **2**, **12** and **14**) as well as C(4) chains within the compounds **3**, **5**, **7**, **9**, **11** (1D packing similarity in pairs with **7** – SC₁ construct). All observed low-dimensional motifs correspond to hydrogen bond patterns, supporting the idea on the structure-forming role of hydrogen bond in crystals. Compound **1**, which does not form hydrogen bonds, has completely different molecular arrangement in crystal compared to other substances.

Based on the available data on different isostructural motifs, two crystal packing families can be built in a way presented in Scheme 3. It is clearly seen that the introduction of two bulky methyl fragments into the adamantane ring leads to significant difference in crystal structures, with no common supramolecular constructs between the derivatives of adamantane and memantine. Compound **7** with the unique C2/c space group still has the similar to other substituted adamantanes arrangement of molecules in hydrogen-bonded chains. The same synthon isostructurality is observed for P2₁/c and P2₁/n crystals of memantine derivatives.

Comparing the structural motifs in considered crystals with the ones already known in the literature, one should have in mind the differences in molecular geometry. The conformation of sulfonamides is bent due to pyramidal orientation of the -SO₂- group, while the molecules of carboxamide and thiourea derivatives are essentially planar. Therefore, XPac could not find any packing similarity between the compounds presented in this article and the ones found in CSD except a few occasional adamantane-to-adamantane dimers.

3.2. Analysis of non-covalent interactions in crystals

3.2.1. Pattern of non-covalent interactions in crystals. At the next stage, solid-state DFT calculations followed by Bader analysis of theoretical periodic electron density were performed to quantify the contributions into the lattice stabilisation from different functional groups and packing motifs. A set of (3;-1) bond critical points corresponding to particular non-covalent interactions has been found for each crystal. The results are presented in Tables 2-14SI.

QTAIMC analysis reveals that the molecules of all considered compounds contain an intramolecular C-H...O contact between the adamantane core and one of oxygen atoms of the sulfo group (Figure 11SI), characterised by a (3;-1) critical point with $\rho_b = 0.009 \div 0.015$ a.u. The energy of this contact lies between 9-13 kJ·mol⁻¹ (absolute value) and increases with the increase of interplanar angle Ph-Ad between phenyl and adamantane fragments, since the bond angle $\angle(\text{C-H-O})$ becomes closer to 180° (Figure 12SI). For molecules **1**, **3**, **7**, **9**, **11**, **12** a short intramolecular C-H... π contact between phenyl and adamantane fragments is also observed with the energy of 3-6 kJ·mol⁻¹. The strength of this interaction is higher for molecules with lower angle between the planes Ph-Ad in the molecule ($R^2 = 0.89$) (Figure 12SI), which can be easily

explained by shortening of the H...C distance between the contact atoms. Similar trend can be observed for intramolecular C-H...O contacts, however, the pair correlation coefficient is lower in this case, since the hydrogen-bonding activity of C-H groups in the phenyl ring also depends on the substituent R.

In the section 3.1 we have supposed that the strength and topology of hydrogen bonds in crystal affects the conformation of the molecule. Basing on the calculated local density of kinetic energy at the (3;-1) critical point obtained from the solid-state DFT, the energies of N-H...O hydrogen bonds were determined using the equation (3). Compared to the estimation of hydrogen bond strength using the equation (2), this approach yields 35-55% higher values of E_{HB} (Table 2). Such difference is expected, since QTAIMC is performed on the periodic wavefunction taken from DFT calculations and therefore takes into account the effects of crystal environment, in contrast to the empirical equation (2). At the same time, a similar regularity is observed between the energies of dimeric and chain-like hydrogen bonding motifs. The average hydrogen bond energy in the dimers is higher than in chain structures (23 kJ·mol⁻¹ against 18 kJ·mol⁻¹ according to QTAIMC) (Table 2). It is easy to trace the dependence between the N...O distance in crystal and the hydrogen bond energy evaluated from Mayo force field and from QTAIMC (Figure 13SI). Only three compounds (**6**, **7** and **11**) do not fit in the considered correlations. This may be caused by the significant deformation of the $\angle(\text{N-H-O})$ bond angle in crystals of **6** and **11** (146.2° и 130.0°, respectively) and higher R-factor compared to other crystals for structure **7** ($R[F^2 > 2\sigma(F^2)] = 6.87\%$).

As an alternative method of examination of the properties of non-covalent interactions in crystals, Hirshfeld surface analysis was performed. It was found that the minimum value of the descriptor d_{norm} in the hydrogen bonding area determined by Hirshfeld surface analysis, correlates linearly with the N...O distance in crystal (Figure 14SI). The similar nature of the dependencies presented in Figure 14SI and Figure 3, allows using the quantity $d_{\text{norm}}^{\text{min}}(\text{HB})$ as a descriptor for estimation of hydrogen bonding energy derived using the Mayo equation and QTAIMC analysis with accuracy greater than 1 kJ·mol⁻¹. (Figure 15SI).

Aside the N-H...O hydrogen bond, the stabilisation of molecules in the main synthon for most structures comes from the formation of additional C-H...O bonds with the proximate hydrogen atom of adamantane cage (in the case of chain motifs) or phenyl ring (in case of dimeric organisation) presented in Figure 7. The energy of these interactions is nearly constant for adamantanes (7-9 kJ·mol⁻¹) and changes significantly from crystal to crystal within the row of memantine derivatives (3-9 kJ·mol⁻¹). The mutual orientation of molecules within a single chain also promotes the formation of a short C-H...N contact with the energy of 5-7 kJ·mol⁻¹ in adamantane-based compounds (2 kJ·mol⁻¹ in compound **1**, which does not form hydrogen bonds). This interaction is absent in crystals of memantine-substituted molecules which form centrosymmetric dimers. The topology of intermolecular

ARTICLE

Journal Name

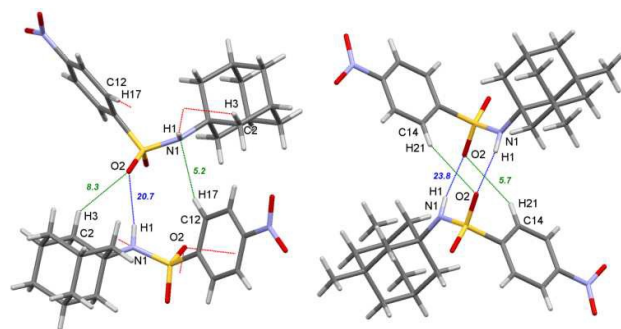


Figure 7. Examples of intermolecular interactions building hydrogen-bonded synthons of two different types: infinite chain in compound **9** (a) and isolated dimer in compound **10** (b). Coloured numbers represent the interaction energies of hydrogen bonds (blue) and C-H...O/N contacts (green) estimated from QTAIMC in $\text{kJ}\cdot\text{mol}^{-1}$.

interactions in the synthon can be demonstrated using the pair of compounds **9** and **10** with para-nitro substituent in the phenyl ring (Figure 7). In addition to already named C-H...O and C-H...N contacts, the oxygen atom in crystals **5** and **7** is also coordinated by the weaker interactions with total energy 4.7 and 10.3 $\text{kJ}\cdot\text{mol}^{-1}$, respectively. Hence, the total energy of non-covalent interactions within the chain motif exceeds the interaction energy within the dimer (average value is 36 against 28 $\text{kJ}\cdot\text{mol}^{-1}$).

The assessment of stabilisation energies coming from the satellite C-H...O contacts sheds the light on the formation of chain-like motifs in crystals of compounds in Table 1SI where adamantane fragment is bound to the carboxamide moiety and the dimer-like motifs in thiourea derivatives. Indeed, as the van-der-Waals radius of the sulfur atom is greater than one of carbon, it can accept more C-H...S contacts to stabilise the dimeric structure. A simple evaluation of C-H...S contacts can be made basing only on metric criteria; however, a thorough QTAIM analysis is needed to be performed for a more reasonable conclusion.

It is interesting to note that the isolated N-H...O bond contributes only 10-20% into the lattice energy, which is lower than its satellite C-H...O contacts in adamantane-based compounds (Figure 8). The fact that crystal **1** with no conventional N-H...O hydrogen bonds in the structure has sublimation enthalpy close to other compounds in the row^{21, 22} also suggests that hydrogen bonds do not contribute significantly to the stabilisation of crystal structure. The possible explanation of this phenomenon can be the domination of H...H contacts, so a structure without any hydrogen bonds would be more thermodynamically preferable. Other crystals with N-H group not linked to the hydrogen bond acceptor include HALQER⁵⁴ and HUGYAK⁵⁵. The common feature of these compounds is the absence of free strong hydrogen bond-accepting substituents not involved into intramolecular bonds.

25% to 50% of non-covalent interaction energy comes from close H...H contacts (Figure 8). This type of interactions dominates in crystals of adamantane-substituted compounds. There are many evidences of attractive nature of 'hydrophobic' intermolecular H...H interactions and their significance for

stabilisation of the crystal lattice present in the literature⁵⁶. In present work, the use of Grimme's D2 dispersion correction³² leads to increase of electron density in the H...H contact area and the number of distinguishable bond critical points, providing a more detailed description of this interaction type. It is noteworthy that the average energy of interaction between two nearest adamantane fragments in crystal estimated using QTAIMC is significantly higher than the dissociation of isolated adamantane dimer⁵⁷ (12 versus 6.4 $\text{kJ}\cdot\text{mol}^{-1}$). We suppose that this example illustrates the effect of crystal environment on the non-covalent interaction energy, since the H...H distances in considered crystals are significantly shorter than in the gas-phase dimer.

Aside from primary synthons and close contacts, the lattices of studied molecules contain the C-H...O contacts, where phenyl and adamantane fragments act as donors and oxygen atoms of sulfonamide group as well as nitro group in compounds **9** and **10**. IUPAC includes these interactions into the class of hydrogen bonds, highlighting their role in stabilisation of supramolecular structures.⁵⁸ The energies of these interactions vary between 3 and 7 $\text{kJ}\cdot\text{mol}^{-1}$ and depend on electron donating or electron withdrawing nature of substituent in the phenyl ring (Figure 8). The shortest and strongest C-H...O contacts are observed in structures containing electron withdrawing groups in the para-position (-Hal, -CF₃, -NO₂). Their energy can reach up to 9 $\text{kJ}\cdot\text{mol}^{-1}$.

The Hirshfeld surface analysis performed in paper by Saeed et al.¹⁸ yields in general close results, with H...H contacts and hydrogen bonds acting as the main stabilising forces in the crystal. Similar conclusions can be made from the comparative analysis of the contributions into the PIXEL lattice energy performed in the work by Al-Wahaibi et al.⁵

In the crystals of halogen-substituted compounds **3-6**, **14**, the C-H...Hal contacts build about 8-10% of total lattice energy and up to 20% for compounds **7** and **8** with -CF₃ fragments (Table 14 SI). Bader analysis also reveals weak (total energy does not exceed 7 $\text{kJ}\cdot\text{mol}^{-1}$) contacts Hal...X, where X = C, O or N. It is

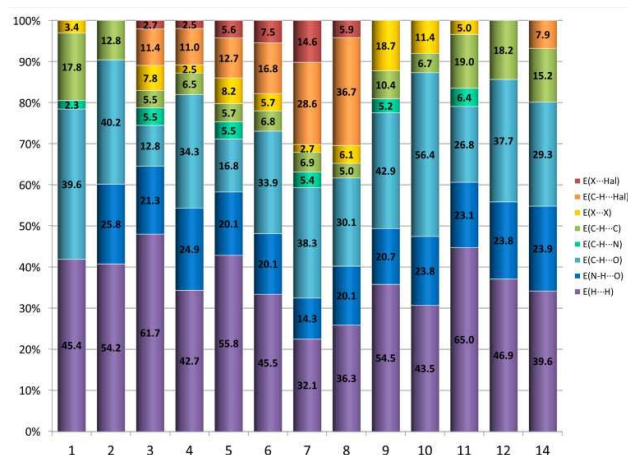


Figure 8. Energies of intermolecular interactions between different atom types in studied compounds calculated by QTAIMC plotted as percentages of lattice energy. The numbers display the total contribution of the interaction in $\text{kJ}\cdot\text{mol}^{-1}$. X stands for C, N, and O atoms.

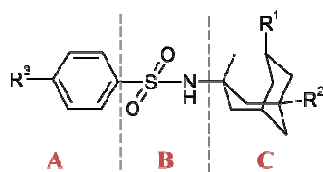
also interesting to consider the crystal **7** with C2/c symmetry, where close packing of $-\text{CF}_3$ groups causes the F...F interaction to form with energy equal to $8.2 \text{ kJ}\cdot\text{mol}^{-1}$. At the same time, the contribution of C-H...O contacts decreases due to the competition between acceptor sites as well as steric hindrances. Similar effect was observed by Al-Wahaibi et al.⁵ upon introduction of the fluorine atom into the molecule of the isothiourea derivative, when the F...F contacts partially replaced H...H contacts in the fingerprint plot of the Hirshfeld surface.

Generally, the introduction of halogen atoms and halogen-containing groups does not lead to significant changes in total lattice energy compared to other substituents except the structures **7** and **8**, where the total contribution from the interactions involving fluorine atoms equals $43 \text{ kJ}\cdot\text{mol}^{-1}$, or 30% of E_{latt} value. Though, it should be noted that the precise description of non-covalent interactions involving halogen atoms (especially Hal...X and Hal...Hal) using the DFT calculations with Gaussian-type orbitals requires the use of diffuse orbitals, the use of which in solid-state calculations is not straightforward and may lead to problems with SCF convergence. As a result, the impact of Hal atoms on theoretical crystal lattice energy can be significantly overestimated.

According to Etter's rules, stronger hydrogen bond donors tend to interact with stronger acceptors⁵⁹. For this reason, as well as due to conformation hindrances, the donors of strong C-H...X (X = O, Hal) contacts with energy above $5 \text{ kJ}\cdot\text{mol}^{-1}$ usually are more polarised C-H groups in the aromatic ring, while weaker C-H...X bonds ($E_{\text{int}} < 5 \text{ kJ}\cdot\text{mol}^{-1}$) and C-H... π interactions are formed are formed by donor groups of the adamantane cage.

3.2.2. The influence of different molecular fragments on the energy of non-covalent interactions in crystal. Let us consider the impact of different functional groups on the energy of non-covalent interactions in studied crystals. For this purpose we conventionally split the molecule into three fragments: fragment **A**, which consists of phenyl ring with substituent R, fragment **B**, which includes the sulfonamide group, and fragment **C**, equivalent to adamantane/memantine cage (Scheme 4). Thus, we get six components of lattice energy, which describe different interaction types governing the molecular packing. In particular, the **B-B** contribution shows the fraction of N-H...O hydrogen bonding, and **C-C** contribution represents the efficiency of packing of adamantane/memantine fragments in crystal.

Total contribution from the **A-C** interactions, which reflects the mutual affinity of phenyl ring and adamantane fragment, is



Scheme 4. A scheme showing the division of molecule into three conventional fragments.

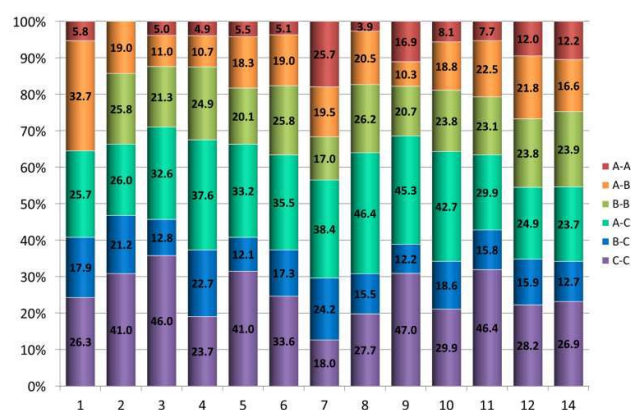


Figure 9. Energies of intermolecular interactions between different fragments in studied compounds calculated by QTAIMC plotted as percentages of lattice energy. The numbers display the total contribution of the interaction in $\text{kJ}\cdot\text{mol}^{-1}$. For fragment numeration, see Scheme 4.

considerably higher in compounds containing in their structure bulky electron donating groups capable of participating in C-H...X contacts such as $-\text{NO}_2$ and $-\text{CF}_3$ ($\Sigma E_{\text{int}}(\text{A-C}) = 38\text{--}46 \text{ kJ}\cdot\text{mol}^{-1}$), less in compounds with $-\text{Cl}$ and $-\text{Br}$ fragments ($32\text{--}38 \text{ kJ}\cdot\text{mol}^{-1}$) and minimal in crystals with R = $-\text{H}$, $-\text{CH}_3$ and $-\text{F}$ ($24\text{--}30 \text{ kJ}\cdot\text{mol}^{-1}$) (Figure 9).

Whereas the contribution of interactions involving fragment **A** is mostly determined by nature of the substituent in the phenyl ring, the energy of interactions of fragment **C** with surroundings depends more on molecular packing. Of three sets of isostructural crystals described above, the layered packing in crystals **3**, **5**, **9**, **11** with P2₁/c symmetry is most efficient from the point of energetic contributions into the lattice energy ($\Sigma E_{\text{int}}(\text{C-C}) = 41\text{--}47 \text{ kJ}\cdot\text{mol}^{-1}$) (Figure 9). This arrangement is observed only for compounds with adamantane fragment. However, adamantane derivatives **1** and **7** crystallise in different space groups and display substantially lower contribution of fragment **C** into the lattice energy. Less energetically favourable packing of memantine cages in isostructural crystals **4**, **6**, **8**, **10** ($\Sigma E_{\text{int}}(\text{C-C}) = 24\text{--}34 \text{ kJ}\cdot\text{mol}^{-1}$) is partially compensated by interactions of methyl groups with fragments **A** and **B** of adjacent molecules, leading to the contribution of fragment **C** equal to 42–44% of the E_{latt} . For comparison, in the set consisting of **3**, **5**, **9**, **11** this value lies in the range 47–53%. Finally, the least efficient packing of memantine fragments (38–39% of E_{latt} value) is observed for crystals **12** and **14** with P2₁/n symmetry.

The close breakdown of lattice energy into main contributions from intermolecular interactions is observed in Hirshfeld surface analysis. According to this approach, the main contribution into the crystal lattice comes from dispersive H...H interactions, which build from 41% to 72% of Hirshfeld surface area (Figure 10). The H...O contacts including the N-H...O and C-H...O hydrogen bonds are on the second place. These contacts occupy approximately 18% of surface area for most crystals and twice as more for the compounds **9** and **10** with $-\text{NO}_2$ fragment. For the crystals containing halogen atoms, a significant contribution comes from the H...Hal interactions

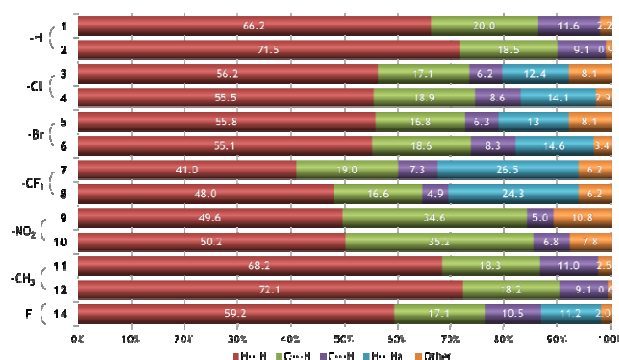


Figure 10. Main contributions of intermolecular contacts between atoms of different types into the Hirshfeld surface for individual molecules within the crystal structures of the compounds under study.

(above 10%). Other weaker interactions present in crystal include the Hal...C/O (1-4%) contacts also visible in QTAIMC analysis and weak C-H...N bonds (0.7-3%) observed only in adamantane derivatives. For the compounds containing the nitro group, uncommon O...O and C...O contacts are present and build up to 6% of total Hirshfeld surface. C...C contacts are nearly absent in all considered crystal structures, which indicates the negligibly small influence of π -stacking on the stability of the crystal structure. These results are in a good agreement with data obtained by Saeed et al.¹⁸ on six structurally relative adamantane-substituted thioureas.

The contributions of interactions of different types into the Hirshfeld surface significantly depend on substituent type, as presented in Figure 10. Within the pairs of compounds with the same substituent in the phenyl ring, the memantine derivatives mostly have higher percentage of H...H interactions. The crystals with similar substituents (halogen atoms in structures **3**, **4**, **5**, **6**, **14**) also have similar distribution of contacts. An unusually high contribution of contacts involving halogen atoms is observed in structures of CF₃-substituted compounds **7** and **8**. Additionally, compound **7** forms a unique intermolecular F...F contact which is absent in other crystals. QTAIMC analysis also reveals this interaction. In crystals of molecules **1**, **2**, **11**, **12**, which contain in their structure no substituents capable of specific bonding, the fraction of H...H contacts is increased.

Fingerprint plots presented in Figures 16SI and 17SI can also provide some information on the nature of non-covalent interactions and their relative strength. The position and size of the side bonding areas in the plot of H...O contacts corresponding to weak (d_i , $d_e \geq 1.6$ Å) C-H...O contacts indicate the ratio of this interactions in the lattice energy. Characteristic lateral areas, corresponding to specific H...Hal contacts, are shifted into the region of smaller distances for shorter H...F contacts and toward the far region for contacts with more bulky atoms Cl and Br. The size and position of these areas indicates the bonding energy in these contacts.

Conclusions

Six new derivatives of sulfonamides with adamantane and memantine substituents were synthesised and characterised by ¹H and ¹³C NMR, FT-IR, DSC and element analysis, their single crystals were grown and crystal structures determined. All adamantane derivatives excluding the unsubstituted compound **1** have the C(4) hydrogen-bonded chains in their crystal structures, while memantine derivatives display the R₂²(8) dimer organisation of hydrogen bonds possibly due to steric hindrances. The energies of N-H...O hydrogen bonds in chain motifs estimated by QTAIMC and Mayo equation are found to be lower than in dimers. Taking into account the satellite C-H...O contacts, the total synthon energy behaves in the opposite manner, with C(4) chains being more energetically preferable, in agreement with synthon occurrence for relative compounds in the CSD. A correlation between the estimated energies of N-H...O hydrogen bonds and the minimal d_{norm} parameter in the bonding area was also established.

The dependence of packing efficiency on the nature of the substituent in the phenyl ring compared to unsubstituted parent compounds was studied with the help of the introduced β -parameter. It was found that the introduction of -Cl, -NO₂ and -Br fragments increase the molecular packing density in crystal of both adamantane and memantine derivatives, while the bulky -CF₃ fragment has the opposite effect.

XPac analysis has revealed three sets of crystals with the established 3D isostructurality with different packing arrangement of phenyl and adamantane fragments. No common supramolecular constructs were found between the adamantane and memantine derivatives, while the OD (dimer) and 1D (chain) hydrogen-bonded motifs persist for all compounds within these packing families.

Solid-state DFT calculations followed by QTAIMC analysis of periodic electron density and Hirshfeld surface analysis allowed us to quantify the non-covalent interactions in crystals and their contribution into the lattice energy. The main contributions into the lattice energy are dispersive H...H contacts and weak hydrogen bonds. The layered packing of adamantane fragments in the group of isostructural adamantane derivatives with P2₁/c symmetry was found to be the most efficient, while the group of memantine derivatives with P2₁/n symmetry demonstrates the least energetically favourable packing type.

Conflicts of interest

There are no conflicts to declare.

Acknowledgements

The synthetic part of the work has been done within the framework of 2018 year National Program (№ 0090-2017-0023). Crystallographic and theoretic parts of the work have been done within the framework of 2018 year National

Program (№ 0092-2014-0005). We thank “the Upper Volga Region Centre of Physicochemical Research” for technical assistance with the XRPD experiments. X-ray diffraction studies were performed at the Centre of Shared Equipment of IGIC RAS.

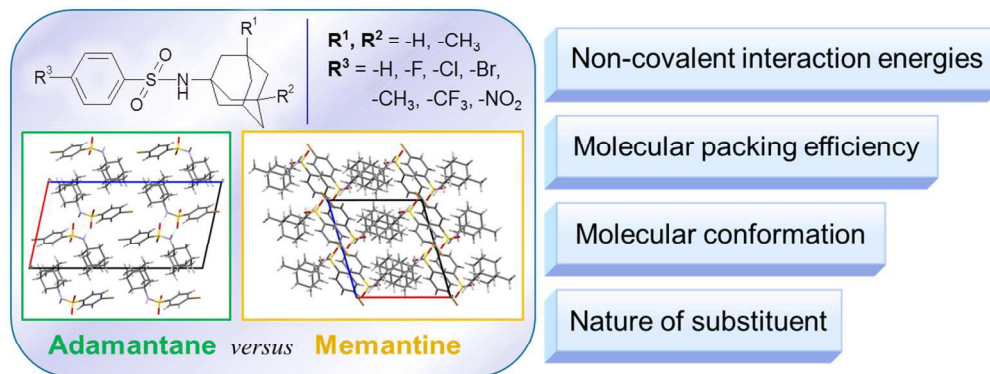
Notes and references

- J. Drew, *Science*, 2000, **287**, 1960-1964.
- T. Owa and T. Nagasu, *Exp. Opin. Ther. Patents*, 2000, **10**, 1725-1740.
- C. W. Thornber, *Chem. Soc. Rev.*, 1979, **8**, 563-580.
- A. E. Boyd, *Diabetes*, 1988, **37**, 847-850.
- L. H. Al-Wahaibi, H. M. Hassan, A. M. Abo-Kamar, H. A. Ghabbour and A. A. El-Emam, *Molecules*, 2017, **22**, 710-722.
- A. A. El-Emam, K. A. Alrashood, M. A. Al-Omar and A.-M. S. Al-Tamimi, *Molecules*, 2012, **17**, 3475-3483.
- C. T. Supuran and A. Scozzafava, *Exp. Opin. Ther. Patents*, 2002, **12**, 217-242.
- C. T. Supuran, A. Scozzafava and A. Casini, *Med. Res. Rev.*, 2003, **23**, 146-189.
- G. S. Hassana, A. A. El-Emam, L. M. Gad and A. E. M. Barghash, *Saudi Pharm. J.*, 2010, **18**, 123-128.
- C. T. Supuran and A. Scozzafava, *Exp. Opin. Ther. Patents*, 2000, **10**, 575-600.
- R. C. Ogden and C. W. Flexner, *Protease Inhibitors in AIDS Therapy*; Marcel Dekker: New York, 2001.
- C. T. Supuran, A. Scozzafava and B. W. Clare, *Med. Res. Rev.*, 2002, **22**, 329-372.
- A. Scozzafava and C. T. Supuran, *J. Med. Chem.*, 2000, **43**, 3677-3687.
- K. Spilovska, F. Zemek, J. Korabecny, E. Nepovimova, O. Soukup, M. Windisch and K. Kuca, *Curr. Med. Chem.*, 2016, **23**, 3245-3266.
- A. Stimac, M. Sekutor, K. Mlinaric-Majerski, L. Frkanec and R. Frkanec, *Molecules*, 2017, **22**, 297.
- É. A. Shokova and V. V. Kovalev, *Pharm. Chem. J.*, 2016, **50**, 3-15.
- J. Liu, D. Obando, V. Liao, T. Lifa and R. Codd, *Eur. J. Med. Chem.*, 2011, **46**, 1949-1963.
- A. Saeed, M. Bolte, M. F. Erben and H. Pérez, *CrystEngComm*, 2015, **17**, 7551-7563.
- G. L. Perlovich, N. N. Strakhova, V. P. Kazachenko, T. V. Volkova, V. V. Tkachev, K.-J. Schaper and O. A. Raevsky, *Int. J. Pharm.*, 2008, **349**, 300-313.
- G. L. Perlovich, A. M. Ryzhakov, V. V. Tkachev, L. Kr. Hansen and O. A. Raevsky, *Cryst. Growth Des.*, 2013, **13**, 4002-4016.
- G. L. Perlovich, A. M. Ryzhakov, V. V. Tkachev and A. N. Proshin, *CrystEngComm*, 2015, **17**, 753-763.
- G. L. Perlovich, T. V. Volkova, A. V. Sharapova, V. P. Kazachenko, N. N. Strakhova and A. N. Proshin, *PCCP*, 2016, **18**, 9281-9294.
- Bruker (2007). APEX2 and SAINT. Bruker AXS Inc., Madison, Wisconsin, USA.
- G. M. Sheldrick, SADABS. University of Göttingen, Germany, 1997.
- Oxford Diffraction (2009). *CrysAlis CCD* and *CrysAlis RED* Oxford Diffraction Ltd, Yarnton, England.
- G. M. Sheldrick. Crystal structure refinement with SHELXL. *Acta Cryst.*, 2015, **C71**, 3-8.
- J. L. Pascual-Ahuir and E. Silla, *J. Comput. Chem.*, 1990, **11**, 1047-1060.
- T. Gelbrich, D. S. Hughes, M. B. Hursthouse and T. L. Threlfall, *CrystEngComm*, 2008, **10**, 1328-1334.
- S. L. Mayo, B. D. Olafson and W. A. Goddard III, *J. Phys. Chem.*, 1990, **94**, 8897-8909.
- R. Dovesi, R. Orlando, A. Erba, C. M. Zicovich-Wilson, B. Civalieri, S. Casassa, L. Maschio, M. Ferrabone, M. De La Pierre, P. D'Arco, Y. Noël, M. Causà, M. Rérat and B. Kirtman, *Int. J. Quantum Chem.*, 2014, **114**, 1287-1317.
- S. A. Katsyuba, M. V. Vener, E. E. Zvereva, Z. Fei, R. Scopelliti, J. G. Brandenburg, S. Siankevich and P. J. Dyson, *J. Phys. Chem. Lett.*, 2015, **6**, 4431-4436.
- S. J. Grimme, *J. Comput. Chem.*, 2006, **27**, 1787-1799.
- R. F. W. Bader, *Atoms in Molecules - A Quantum Theory*. Oxford University Press: Oxford, 1990.
- V. G. Tsirelson and R. P. Ozerov, *Electron Density and Bonding in Crystals*. Bristol, England / Philadelphia, USA: Institute of Physics Publishing, 1996.
- C. Gatti and S. Casassa, *TOPOND14 User's Manual*, CNR-ISTM Milano, Milano, 2014.
- I. Mata, I. Alkorta, E. Espinosa and E. Molins, *Chem. Phys. Lett.*, 2011, **507**, 185-189.
- M. V. Vener, E. O. Levina, O. A. Koloskov, A. A. Rykounov, A. P. Voronin and V. G. Tsirelson, *Cryst. Growth Des.*, 2014, **14**, 4997-5003.
- P. M. Dominiak, E. Espinosa and J. Ángyán, In *Modern Charge Density Analysis*; Editors: C. Gatti and P. Macchi, Springer, Heidelberg, 2012, 387-433.
- Y. A. Abramov, A. Volkov, G. Wu and P. Coppens, *J. Phys. Chem. B*, 2000, **104**, 2183-2188.
- A. N. Manin, A. P. Voronin, A. V. Shishkina, M. V. Vener, A. V. Churakov and G. L. Perlovich, *J. Phys. Chem. B*, 2015, **119**, 10466-10477.
- A. O. Surov, A. V. Churakov and G. L. Perlovich, *Cryst. Growth & Des.*, 2016, **16**, 6556-6567.
- M. A. Spackman and D. Jayatilaka, *CrystEngComm*, 2009, **11**, 19-32.
- S. K. Wolff, D. J. Grimwood, J. J. McKinnon, M. J. Turner, D. Jayatilaka and M. A. Spackman, *CrystalExplorer*, Version 3.1. University of Western Australia, Crawley, Australia, 2012.
- J. J. McKinnon, D. Jayatilaka and M. A. Spackman, *Chem. Commun.*, 2007, 3814-3816.
- A. Saeed, M. F. Erben and M. Bolte, *Spectrochim. Acta A*, 2013, **102**, 408-413.
- A. Saeed, U. Florke and M. F. Erben, *J. Mol. Struct.*, 2014, **1065**, 150-159.
- A. Saeed, Z. Ashraf and M. F. Erben, *J. Simpson, J. Mol. Struct.*, 2017, **1129**, 283-291.
- M. C. Etter, J. C. McDonald and J. Bernstein, *Acta Cryst.* 1990, **B46**, 256-262.
- J. Bernstein, R. E. Davis, L. Shimoni and N.-L. Chang, *Angew. Chem. Int. Ed. Engl.*, 1995, **34**, 1555-1573.
- H.-H. Prohl, A. Blaschette and P. G. Jones, *Acta Cryst.*, 1997, **C53**, 1434-1436.
- L. Wanka, C. Cabrele, M. Vanejews and P. R. Schreiner, *Eur. J. Org. Chem.*, 2007, 1474-1490.
- R. Hrdina, F. M. Metz, M. Larrosa, J.-P. Berndt, Y. Y. Zhygadlo, S. Becker and J. Becker, *Eur. J. Org. Chem.*, 2015, 6231-6236.
- T. L. Threlfall and M. B. Hursthouse, *CrystEngComm*, 2012, **14**, 5454-5464.
- J. K. Maurin, W. Lasek, A. Gorska, T. Switaj, A. B. Jakubowska and Z. Kazimierczuk, *Chem. Biodiversity*, 2004, **1**, 1498-1512.
- A. A. Fokin, A. Merz, N. A. Fokina, H. Schwertfeger, S. L. Liu, J. E. P. Dahl, R. M. K. Carlson and P. R. Schreiner, *Synthesis*, 2009, 909-912.
- M. V. Vener, A. N. Egorova, D. P. Fomin and V. G. Tsirelson, *J. Phys. Org. Chem.*, 2009, **22**, 177-185.
- J. Echeverría, G. Aullón, D. Danovich, S. Shaik and S. Alvarez, *Nature Chemistry*, 2011, **3**, 323-330.
- E. Arunan, G. Desiraju, R. Klein, J. Sadlej, S. Scheiner, I. Alkorta, D. C. Clary, R. H. Crabtree, J. J. Dannenberg, P.

ARTICLE

Journal Name

- Hobza, H. G. Kjaergaard, A. C. Legon, B. Mennucci and D. J. Nesbitt, *Pure and Appl. Chem.*, 2011, **83**, 1619-1636.
59 M. C. Etter, *Acc. Chem. Res.* 1990, **23**, 120-126.



159x79mm (300 x 300 DPI)